\$ SUPER

Contents lists available at ScienceDirect

Ecological Indicators

journal homepage: www.elsevier.com/locate/ecolind



Original Articles

Comparison of vegetation responses to diverse water sources in the Yangtze River Basin: Insights from meteorological, hydrological, and agricultural drought

Sijing Cui ^{a,b}, Jun Gao ^{a,b}, Fengyun Sun ^{a,b,*}, Gen Li ^c, Yue Che ^d

- ^a School of Environmental and Geographical Sciences, Shanghai Normal University, Shanghai 200234, China
- ^b Yangtze River Delta Urban Wetland Ecosystem National Field Scientific Observation and Research Station, Shanghai 200234, China
- ^c Research Center for Monitoring and Environmental Sciences, Taihu Basin & East China Sea Ecological Environment Supervision and Administration Authority, Ministry of Ecology and Environment, Shanghai 200125, China
- ^d School of Ecological and Environmental Sciences, East China Normal University, Shanghai 200241, China

ARTICLE INFO

Keywords: Water availability Vegetation stress Drought NDVI anomaly Correlation analysis SWAT Yangtze River Basin

ABSTRACT

Understanding the intricate link between water availability and vegetation growth is crucial for preserving ecosystem vitality and facilitating global carbon cycling. The Yangtze River Basin (YRB) features vast subtropical forests, which are vital for global hydrological, carbon, and energy flows. Investigating the influence of the water supply on vegetation dynamics in this basin is crucial, particularly in light of the challenges posed by climate change. However, the response of vegetation to different water sources remains poorly understood. To address this gap, this study explores the influence of precipitation, surface runoff, and soil water on vegetation growth in the YRB via hydrologic modelling and remote sensing data from 2003 to 2021. The results revealed a decreasing trend in drought-prone areas. The overall vegetation growth has progressively improved despite challenges posed by water scarcity. More areas in the YRB are affected by water shortages than surpluses in terms of vegetation growth. During the growing season, vegetation is primarily affected by water shortage, although in exceptional cases, it is constrained by excess water, which typically occurs during the nongrowing season. In the upper and middle Jinsha River Basin, vegetation growth is primarily restricted by water surpluses, while in the middle and lower YRB, constraints commonly arise from water deficits. Additionally, surface runoff and soil moisture play more significant roles in influencing vegetation growth than precipitation. By revealing the dynamics of the vegetation-water correlation, our research aims to provide valuable insights for managing the dynamic balance between water and vegetation in subtropical regions.

1. Introduction

Vegetation growth is influenced by nuanced fluctuations in water availability (Mitchell et al., 2016). As vegetation adapts to these conditions, it triggers physiological responses, affecting hydrological, carbon, and energy flows regionally and globally (Jung et al., 2010; Humphrey et al., 2018). Among temperature, radiation, and water, the latter is considered to have the most significant impact on reducing vegetation productivity under climate change (Nemani et al., 2003; Reichstein et al., 2007). For example, a rapid flood results in nutrient loss from waterlogging (Blom, 1999; Kreuzwieser and Rennenberg, 2014), whereas a flash drought causes functional impairment from water scarcity (Allen et al., 2015). Therefore, considering both excessive

and deficient water is essential for understanding vegetation growth in response to water availability.

More research has focused on the gradual response of vegetation to changes in water availability than on its response to anomalous water supplies (Tang et al., 2024). The vegetation water supply is a complex system that integrates atmospheric, hydrological, and soil moisture processes. However, recent research has focused mostly on vegetation dynamics from the perspective of single water sources, such as precipitation (e.g., Lawal et al., 2019; Smith and Boers, 2023), hydrological runoff (e.g., Peña-Angulo et al., 2021; Seka et al., 2022), and soil moisture (e.g., Chang et al., 2023; Du et al., 2023). Additionally, the response of vegetation to different water supplies remains unclear. This includes the process of vegetation adaptation under external water

^{*} Corresponding author at: School of Environmental and Geographical Sciences, Shanghai Normal University, Shanghai 200234, China. *E-mail address:* fysun@shnu.edu.cn (F. Sun).

pressure, encompassing both the duration and severity of its productivity variations. Given this knowledge gap, we compared how different water sources, including precipitation, surface runoff, and soil water, impact vegetation growth. Furthermore, variations in vegetation water use efficiency, driven by factors such as hydraulic traits (Sperry and Love, 2015; Anderegg et al., 2018) and regional topography (Wang et al., 2021a), pose challenges in the long-term quantification of the relationships between vegetation and available water in large watersheds. While correlations between vegetation indicators and drought indices are commonly used to assess this relationship at regional or broader scales (e.g., Schwalm et al., 2017; Peña-Angulo et al., 2021), these variations complicate the accuracy of such assessments.

The Yangtze River Basin (YRB), one of China's most significant geographical features, stands out globally for its vast subtropical forests (FAO, 2020), which exhibit higher average productivity than forests at similar latitudes and in other Asian tropical regions (Yu et al., 2014). However, severe droughts in subtropical regions often occur unexpectedly early (Ji et al., 2024), and the YRB is considered ecologically fragile (Yang et al., 2024) and is recognized as a climate-sensitive area (Qu et al., 2020). For example, the summer heavy rainfall in the YRB in 2020 caused vegetation root waterlogging and hypoxia due to flooding (Zhou et al., 2021). In contrast, the combined drought-heatwave event in the summer of 2022 led to soil moisture scarcity, resulting in a 300 % increase in affected vegetation area compared to earlier in the year (Liu et al., 2023). Therefore, under climate change, investigating the dynamic impacts of the water supply on vegetation has significant implications for ecological security in the YRB.

Building on the importance of understanding the water supply's impact on vegetation under climate change, this study sheds light on how precipitation, runoff, and soil moisture collectively shape vegetation growth by considering both their individual and interactive effects. The Soil and Water Assessment Tool (SWAT) model was constructed to acquire data on precipitation, runoff, and soil moisture within the YRB. Three water availability indices, the standardized precipitation index (SPI), standardized runoff index (SRI), and standardized soil moisture index (SSI), were subsequently derived from these variables, whereas vegetation anomalies were assessed using standardized deviation derived from remotely-sensed Normalized Difference Vegetation Index (NDVI) data, referred to as SNDVI. Finally, this study links water availability indices with the vegetation index to investigate the spatiotemporal dynamics of the vegetation response to water availability from 2003 to 2021 within the YRB. The findings offer new insights into the relationships between vegetation and available water management, as well as ecological conservation in subtropical regions.

2. Study area and datasets

2.1. Study area

The YRB encompasses a diverse array of microclimates and vegetation ecosystems across its regions, extending from the high-elevation Qinghai–Tibet Plateau in western China to the low-lying Yangtze Plain in the east (Zhang et al., 2022) (Fig. 1). Precipitation in the YRB is strongly influenced by monsoonal patterns, resulting in significantly greater annual precipitation than in regions at similar latitudes (Wei et al., 2020). Moreover, the frequency of heavy precipitation events in the YRB has increased in recent decades (Hu et al., 2021), a trend linked to diminished vegetation productivity (Smith and Boers, 2023). Moreover, the YRB is one of the most biologically diverse and ecologically significant regions in China, encompasses vegetation types from alpine meadows and coniferous forests in the upper basin to subtropical and tropical forests in the lower reaches (Qu et al., 2020). Along riverbanks and floodplains, there are extensive wetlands and marshes, which provide important habitats for wetland vegetation (Yang et al., 2024).

2.2. Vegetation index data

Vegetation growth from 2003 to 2021 was assessed in this study using the Aqua MODIS-derived monthly vegetation product, MYD13A3 v061 (https://lpdaac.usgs.gov/products/myd13a3v061/), with NDVI at a 1 km resolution serving as a proxy. This product is generated using advanced quality control techniques, including enhanced cloud and atmospheric corrections, to improve data reliability and minimize errors, particularly in areas frequently affected by cloud cover and atmospheric interference. Monthly NDVI data is consistently available from 2003, covering all 12 months of the year, with pixel values averaged within each subbasin to obtain values for 125 subbasins. The available water data, obtained through the SWAT model, ends in 2021. To align the datasets, this study focuses on the 2003–2021 period, during which multiple extreme drought events occurred (Zhang et al., 2015; Wang et al., 2020).

2.3. Precipitation, runoff, and soil water data

Precipitation, runoff, and soil water data across the YRB from 2003 to 2021 were obtained from SWAT model, simulated on a daily basis and then averaged to obtain monthly data. The data are structured into 125 subbasins, which are the spatial units that serve as a key organizational framework for outputs in the SWAT model. As a semi-distributed hydrological model, SWAT simulates hydrological processes based on

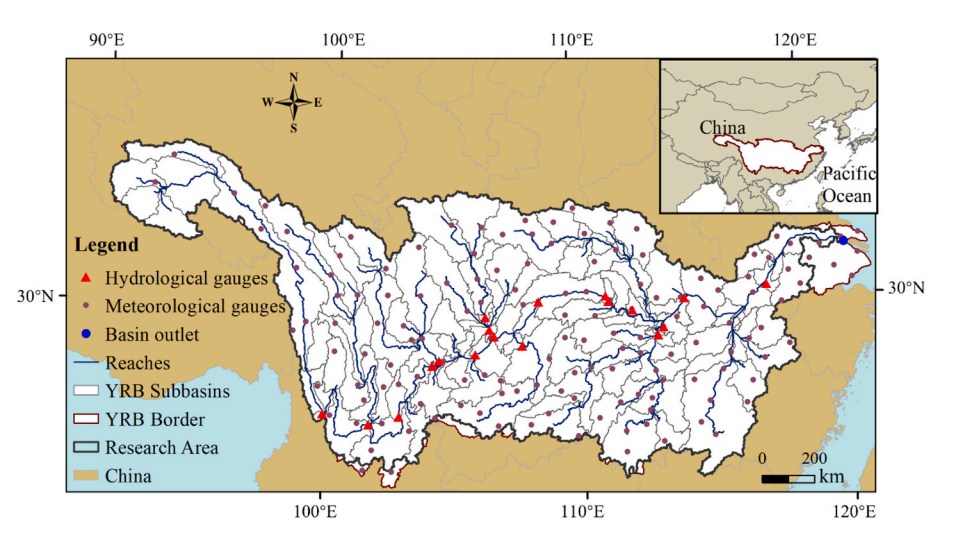


Fig. 1. The geographical distribution of the study area within the YRB.

physical mechanisms and is well-suited for large, complex watersheds (Gassman et al., 2007; Abbaspour et al., 2015). Although SWAT requires extensive data and is sensitive to parameters (Arnold et al., 2012), these features enable it to capture complex hydrological and environmental processes, making it a powerful tool in research on hydrological processes (Douglas-Mankin et al., 2010).

The SWAT modelling system for the YRB was previously developed and applied in studies by Sun et al. (2019) and Zhang et al. (2023a). Details on the model configuration and other specifics are available in these studies, with a brief summary of the data-related aspects in this study provided here. Daily precipitation data from 148 meteorological stations were interpolated into 125 subbasins via the Thiessen polygon method. Daily runoff data for the 125 subbasins were derived from SWAT-simulated streamflow, which includes both surface runoff and subsurface flow transmission to the river channels. Soil moisture data are derived by considering the average root depth of vegetation (Yang et al., 2016), incorporating the heterogeneity of the soil layer, and driven by soil characteristics to estimate infiltration within the 1-meter soil layer. Compared to site monitoring, which cannot provide longterm, large-scale data (Sun et al., 2022), and remote sensing, which is limited to shallow soil moisture (1-5 cm) (Juglea et al., 2010), SWAT offers spatiotemporally continuous soil moisture data at the large watershed scale (Li et al., 2009; Chen et al., 2011).

3. Methodology

3.1. Standardized vegetation anomaly index

In this study, we employ the standardized NDVI (SNDVI) to identify vegetation anomalies. This index removes seasonal effects, enhancing vegetation status assessment and revealing vegetation dynamics. By reflecting the position of the current observation within its historical distribution, it captures and quantifies vegetation anomalies. As such, it is considered a reliable method (Meroni et al., 2019).

The standardized deviation (z score) of the NDVI forms the basis of the SNDVI, as depicted below:

$$Z = \frac{NDVI_i - \mu_i}{S_i} \tag{1}$$

where $NDVI_i$ is the NDVI value for month i from 2003 to 2021, μ_i is the average NDVI for the i month during the study period, and S_i represents the standard deviation of NDVI for the month i and is calculated as follows (2):

$$S_{i} = \sqrt{\frac{1}{n-1} \sum_{i=1}^{n} |NDVI_{ij} - \mu_{i}|^{2}}$$
 (2)

where n = 19 denotes the number of years studied.

A positive value indicates a greater NDVI than the monthly average from 2003 to 2021, suggesting favourable vegetation growth. Conversely, a negative value implies poorer vegetation conditions. Table 1 summarizes the vegetation classification. The SNDVI values are categorized as either below normal or above normal based on specific thresholds, referenced from Meroni et al. (2019), and adjusted to fit the distribution of the annual average SNDVI in the YRB. The distribution

 Table 1

 Specific categorization of vegetation condition.

SNDVI	Vegetation Condition		
−1 to −2	Severely below normal		
−0.5 to −0.99	Moderately below normal		
0 to -0.49	Slightly below normal		
0 to 0.49	Slightly above normal		
0.5 to 0.99	Moderately above normal		
1 to 2	Extremely above normal		

ranges from -2 to 2, with most values concentrated between -1 and 1. A 0.5 interval is applied within the range of -1 to 1 to refine the anomaly distribution, while a 1.0 interval is applied to the range $|x|\in [1,\,2]$ to avoid over-segmentation, aiding in the identification of areas with abnormal vegetation growth or decline.

3.2. Standardized drought index

The Standardized Indices (SI) are simple and effective tools for measuring drought (McKee et al., 1993; Mishra and Singh, 2010). By using a unified statistical approach, they enhance comparability across different water supplies and avoid assumption conflicts between various drought methods (Farahmand and AghaKouchak, 2015), enabling a consistent comparison of vegetation responses to varying moisture conditions. By applying the standardized index method, we calculated monthly water availability indicators, including the SPI (representing meteorological drought), the SRI (indicating hydrological drought), and the SSI (reflecting agricultural drought).

Taking SPI as an example, the process is as follows:

First, the precipitation accumulation P(t) for month t is calculated via Equation (3):

$$P(t) = \sum_{t=2}^{t} w(t),$$
 (3)

where t represents one month over the study period (2003–2021) and where w(t) represents the precipitation data for that month. Then, for each month m over all study years Y, obtain the set of all P(t) values according to Equation (4):

$$S(m) = [P(m), P(1 \times 12 + m), \dots, P((Y - 1) \times 12 + m)], \tag{4}$$

Consequently, S(m) is computed by exercising the empirical Gringorten plotting position, as shown in Equation (5):

$$G_m(r) = \frac{r_m - 0.44}{Y + 0.12},\tag{5}$$

where r_m is the rank of the S(m) value and where $G_m(r)$ is the plotting position of the data sequence r at month m. The cumulative distribution function of $G_m(r)$ can be transformed into a standard normal distribution via the function Φ , as shown in Equation (6):

$$SPI_m = \Phi^{-1}(G_m), \tag{6}$$

where SPI_m represents the standardized precipitation index for month m. The calculations of the SRI and SSI follow a similar procedure as the SPI, replacing precipitation data with runoff and soil moisture data, respectively.

Notably, a 3-month time scale was employed to evaluate short-term water availability in this study because the correlation between the available water index and vegetation index is optimal (Ji and Peters, 2003) for studying the response of vegetation to available water. In assessing drought conditions across the YRB, drought classification is based on the SI values according to McKee et al. (1993). SI values of -1.50 to -1.99 indicate "severe drought", -1.00 to -1.49 represent "moderate drought", 0 to -0.99 denote "mild drought", 0 to 0.99 indicate "mild humidity", and 1.00 to 1.49 signify "moderate humidity".

3.3. Correlation analysis

The Spearman rank correlation method was selected to explore the relationship between vegetation and water availability. This method captures both linear and nonlinear associations (Schober et al., 2018; Hauke and Kossowski, 2011), is well-suited for analysing NDVI anomalies (SNDVI) with SPI, SRI, or SSI without assuming linear correlations. Through Spearman correlation analysis, we derived the correlations between SNDVI and the three indices—SPI, SRI, and SSI—using the

correlation coefficients r(SNDVI, SPI), r(SNDVI, SRI), and r(SNDVI, SSI), respectively.

To compare the effects of different water supplies on vegetation in the YRB, we build upon the framework established by Jiao et al. (2021). We categorize the correlation between SNDVI and water availability indices (SPI, SRI, and SSI) into three distinct scenarios. The first scenario is termed "vegetation water deficit restriction", in which SNDVI shows a significant positive correlation with SPI, SRI, or SSI (p < 0.05). This indicates that an increase in precipitation, runoff, or soil moisture improves vegetation health, whereas a decrease in water supply restricts it. The second scenario is defined as "vegetation water surplus limitation", in which SNDVI exhibits a significant negative correlation with SPI, SRI, or SSI (p < 0.05). In this case, a decrease in precipitation, runoff, or soil moisture enhances vegetation health, while an increase in water availability limits it. The third scenario reflects a lack of significant correlation (p > 0.05), suggesting that vegetation growth is constrained neither by water deficit nor by water surplus in specific regions. This absence of correlation may be attributed to human impacts (Wang et al., 2021b).

3.4. Mann-Kendall (MK) method

To analyse trends in the vegetation–water relationship, we utilize a nonparametric approach, the Mann–Kendall (MK) method (Kendall, 1975), which aids in detecting regional drought and plant cover dynamics. During trend identification, both the MK's tau and the p value should be considered (Sun et al., 2019); hence, five trend categories were taken (see Table 2) to help summarize the trend analysis outcomes. The declining (negative) trends of the vegetation–moisture correlation suggest a preference for vegetation growth to be constrained by water surplus. Conversely, the increasing (positive) trends indicate that vegetation is susceptible to water deficit.

3.5. BRT analysis

To investigate the primary contributors and distinct mechanisms of available water on vegetation growth, we employ the boosted regression tree (BRT) model. This method excels in capturing irregular relationships and is widely used for predicting dependent variables and quantifying their responses (De'ath, 2007; Wu et al., 2020). In our study, the SPI, SRI, and SSI are dimensionless indices obtained through the same methodology, enabling a more precise comparison of their impacts on the SNDVI via R software. We estimated the impact of SPI, SRI, and SSI on SNDVI distributions using the "dismo" package in R and minimized losses to ensure efficiency using the "gbm" package. Testing revealed that for the dataset of vegetation and drought indices, using a learning rate of 0.0001 can steadily improve and capture the true trends. A tree complexity of 5 and a bag fraction of 0.5 ensure computational efficiency and model reliability.

4. Results

4.1. Dynamics of the SPI, SRI, SSI and SNDVI from 2003 to 2021

Combining the SPI, SRI, and SSI, a general decreasing trend is

 Table 2

 Refined Categorization of the MK Trend Analysis Results.

Characteristics	Trend	Symbols	Tau	P value
Strong	decreasing increasing	-2	$\begin{array}{l} \tau < 0 \\ \tau \geq 0 \end{array}$	$p \leq 0.01$
Moderate	decreasing increasing	-1 1	$\begin{array}{l} \tau < 0 \\ \tau \geq 0 \end{array}$	0.01
No sign.	no	0		p > 0.05

observed in drought-prone areas within the YRB from 2003 to 2021. As shown in Fig. 2a–c, mild drought and wetness were prevalent in the YRB during this period. Mild hydrological drought peaked in 2006, affecting approximately 69.92 % of the area (Fig. 2b). In 2013, both mild meteorological and agricultural droughts peaked, impacting approximately 75.70 % and 70.89 % of the region, respectively (Fig. 2a and c).

Under varying drought conditions, the SPI, SRI, and SSI indices show significant differences. In mild drought conditions, the SPI curve exhibits the largest fluctuation amplitude (Fig. 2a). The area of mild drought for SPI reached a maximum of 75.70 %, higher than SRI at 69.92 % and SSI at 70.89 %, and a minimum of 16.29 %, lower than SRI at 20.48 % and SSI at 29.42 % (Fig. 2a–c). In contrast, under moderate drought conditions, the mean areas affected by SRI (4.01 %) and SSI (2.88 %) are larger than those affected by SPI (1.41 %) (Fig. 2a–c). Moreover, mild drought and mild humidity curves show more frequent intersections in SSI, around 12 times, than in SPI (4 times) and SRI (5 times) (Fig. 2a–c).

Overall, vegetation growth in the YRB has gradually improved. From 2003 to 2021, the vegetation status transitioned from negative to positive anomalies, with the area of negative anomalies decreasing from 97.42 % in 2003 to 0.64 % in 2021 (Fig. 2d). Notably, after 2012, positive anomalies became dominant, and in 2013, the area of positive anomalies first surpassed that of negative anomalies, reaching 65.15 % (Fig. 2d). This trend is consistent with the shift in drought status around 2012, transitioning from drought-dominated to nondrought-dominated conditions in the YRB (Fig. 2a–c). Specifically, the average drought area before 2012 in SPI, SRI, and SSI was around 64.42 %, 61.87 %, and 56.82 %, respectively, while in 2012 and the years following, it was around 41.32 %, 40.74 %, and 44.89 %, respectively (Fig. 2a–c).

Most vegetation in the YRB experienced mild anomalies. Specifically, in 2011, slightly negative anomalies peaked, with nearly 65.98 % of the areas showing mildly damaged vegetation (Fig. 2d), whereas slightly positive anomalies peaked in 2014, with approximately 75.79 % of the YRB showing improved vegetation health (Fig. 2d). This is closely related to the moisture supply for vegetation. As shown in Fig. 2a and b, in 2011, both the SPI and SRI drought areas exhibited high values of 70.25~% and 70.06~%, respectively. These values indicate relatively intense drought, characterized by insufficient precipitation and runoff, which contributed to widespread vegetation damage, with around 77.31 % of the vegetation below normal (Fig. 2d). In contrast, in 2014, most basins experienced nondrought conditions. Specifically, the SPI showed 49.91 % of the area as nondrought, the SRI was at 51.92 %, and the SSI at 68.05 % (Fig. 2a-c), with sufficient moisture availability for vegetation recovery, and nearly 84.07 % of the area above normal (Fig. 2d).

4.2. Correlation dynamics between the SNDVI and drought indices

4.2.1. Long-term trend of temporal variation in correlation

We conducted regional statistics on the extent of "vegetation water deficit restriction" (positive correlation, p < 0.05) and "vegetation water surplus limitation" (negative correlation, p < 0.05) in 125 subbasins from 2003 to 2021 (Fig. 3a–c), which included statistical analysis of r (SNDVI, SPI), r(SNDVI, SRI), and r(SNDVI, SSI). To perform trend analysis, we applied a 5-year moving average to smooth the data and used linear regression to identify trends.

In the correlation curves between SNDVI and SPI, SRI, and SSI, the area proportion of vegetation growth under water deficit constraints is generally higher than that under surplus conditions (Fig. 3a–c). Specifically, the constraint of precipitation scarcity on vegetation growth in the YRB shows an upward trend, as indicated by the area proportion where greenery was disturbed by precipitation shortages in the r(SNDVI, SPI) curve, with an annual rate of increase of 0.12 % (Fig. 3a). In contrast, a decreasing trend is observed in the restrictions of runoff and soil moisture deficiency on vegetation productivity in the YRB (Fig. 3b and c). This is reflected in the r(SNDVI, SRI) and r(SNDVI, SSI) curves,

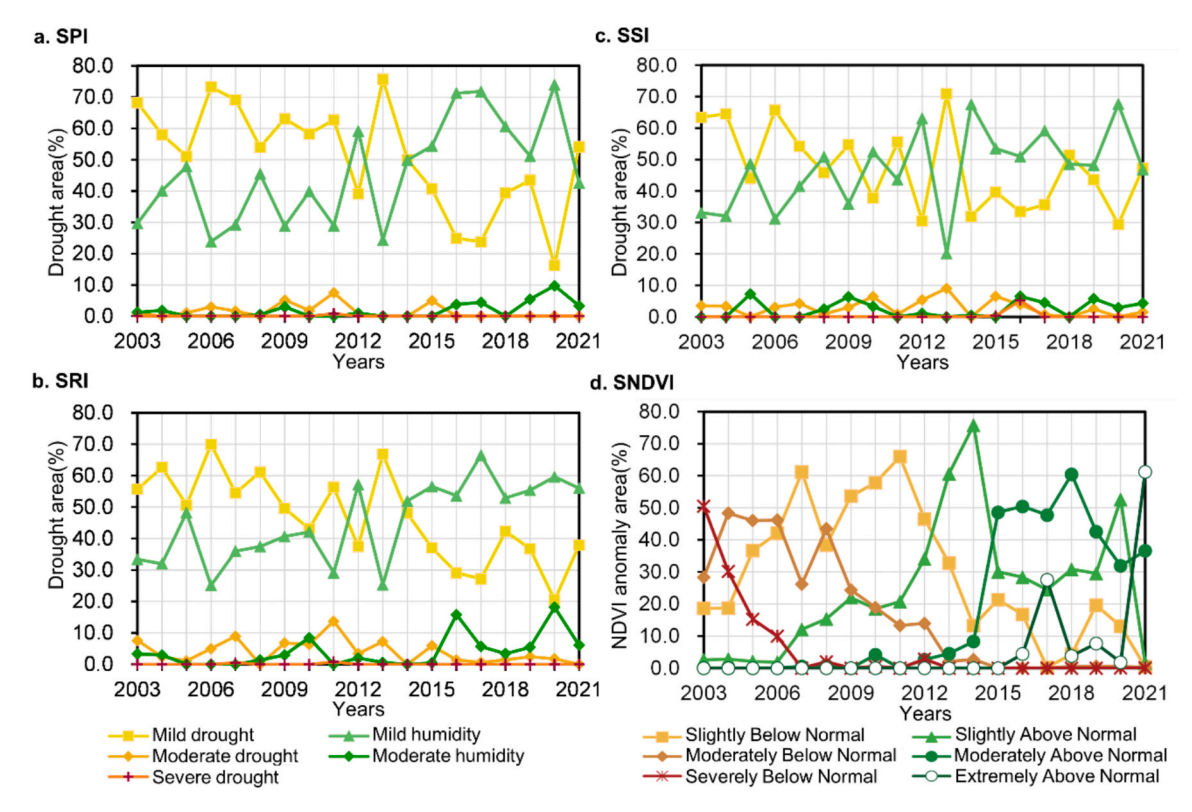


Fig. 2. Drought area percentages and NDVI anomalies in the YRB from 2003 to 2021. Fig. 2a–c illustrate the water supply states of precipitation, runoff, and soil moisture in the YRB, respectively, depicted individually by the SPI (i.e., meteorological drought), SRI (i.e., hydrological drought), and SSI (i.e., agricultural drought). Fig. 2d shows the annual changes in vegetation conditions in the YRB based on the classification of the SNDVI values.

where a downward trend is seen in areas where vegetation is limited by runoff and soil water scarcity, with annual decrease rates in the area proportion of 0.16 % and 0.44 %, respectively (Fig. 3b and c).

Furthermore, the impediment to vegetation vitality by water surplus gradually increased in the YRB, with areas experiencing runoff surplus showing a particularly rapid increase. As shown in Fig. 3a–c, regions where vegetation is restricted by excess water exhibit a gradual but steady upwards trend. Notably, the curve representing the area proportion of vegetation reduction due to precipitation surplus in the r (SNDVI, SPI) exhibited the slowest growth rate, with the affected area proportion increasing by only 0.06 % per year (Fig. 3a). In contrast, the curve indicating the area proportion of vegetation stress caused by runoff surplus in the r(SNDVI, SRI) shows a significant growth rate, supported by an R-squared value of 0.83 and an annual increase of 0.21 % (Fig. 3b).

4.2.2. Short-term fluctuations in temporal variations in correlations

To uncover short-term dynamics and seasonal patterns in the correlation, we examine monthly fluctuations in the relationships between NDVI anomalies (SNDVI) and available water indices (including the SPI, SRI, and SSI) from 2003 to 2021 (Fig. 3d–f).

From April to October, SNDVI showed predominantly positive correlations with available water indices (Fig. 3d–f). Periods during which the available water indices exhibited at least moderate positive correlations with SNDVI (average r>0.37) included July to September 2006 (3 months), August to October 2011 (3 months), July to November 2013 (5 months), and September to December 2019 (4 months). Notably, the latter two periods extended into the winter months (Fig. 3d–f). Among the periods listed above, the positive r(SNDVI, SRI) persisted for the longest duration (Fig. 3d–f). For instance, it extended from July to December in 2006 (6 months), from August to January in 2013 (6 months), and from September to February in 2019 (8 months) (Fig. 3e). Additionally, the r(SNDVI, SSI) exhibited relatively high correlations,

with average r values of 0.55 (July to September 2006), 0.47 (August to October 2011), 0.45 (July to November 2013), and 0.58 (September to December 2019) (Fig. 3f).

However, in exceptional cases during the growing season, SNDVI exhibited negative correlations with available water indices, which typically occur during the nongrowing season. (Fig. 3d–f). Notably, persistent negative correlations between SNDVI and available water indices were observed from May to December 2020, averaging -0.16 in r value (Fig. 3d–f). During this period, r(SNDVI, SRI) showed a stronger negative correlation, primarily in November and December 2020, with an average r value of -0.41. Furthermore, the negative correlation in r (SNDVI, SSI) persisted for the longest duration, lasting from May 2020 to May 2021, totaling 13 months (Fig. 3f).

4.2.3. Characteristics of spatial variation in correlation

To understand the dynamic properties of the correlations in the spatial distribution of the YRB, the MK test was applied across 125 subbasins from 2003 to 2021 (Fig. 4). In the upper YRB, a stronger negative correlation was observed in r(SNDVI, SSI), with a minimum of -0.26 in its sub-basins, compared to r(SNDVI, SPI) and r(SNDVI, SRI), which had minimums of -0.18 and -0.09, respectively (Fig. 4a–c). These correlations primarily located in the upper and middle Jinsha River Basin and the western Min River Basin (Fig. 4a–c). Furthermore, in the upper and middle Jinsha River Basin, a patchy distribution of decreasing trends in r(SNDVI, SSI) was observed (Fig. 4i).

Additionally, more regions in the upper YRB exhibited positive correlations (Fig. 4a–c). In the Source Region of the Yangtze River, stronger positive correlations were observed in r(SNDVI, SPI) and r (SNDVI, SRI), with maximum r-values of 0.15 and 0.27 in its sub-basins, respectively, while r(SNDVI, SSI) showed a weaker positive correlation, peaking at 0.04 (Fig. 4a–c). In the southern basin of the Jinsha River, r (SNDVI, SSI) exhibited a relatively higher positive correlation, reaching a maximum of 0.64 (Fig. 4a–c). Similarly, in the northwestern Jialing

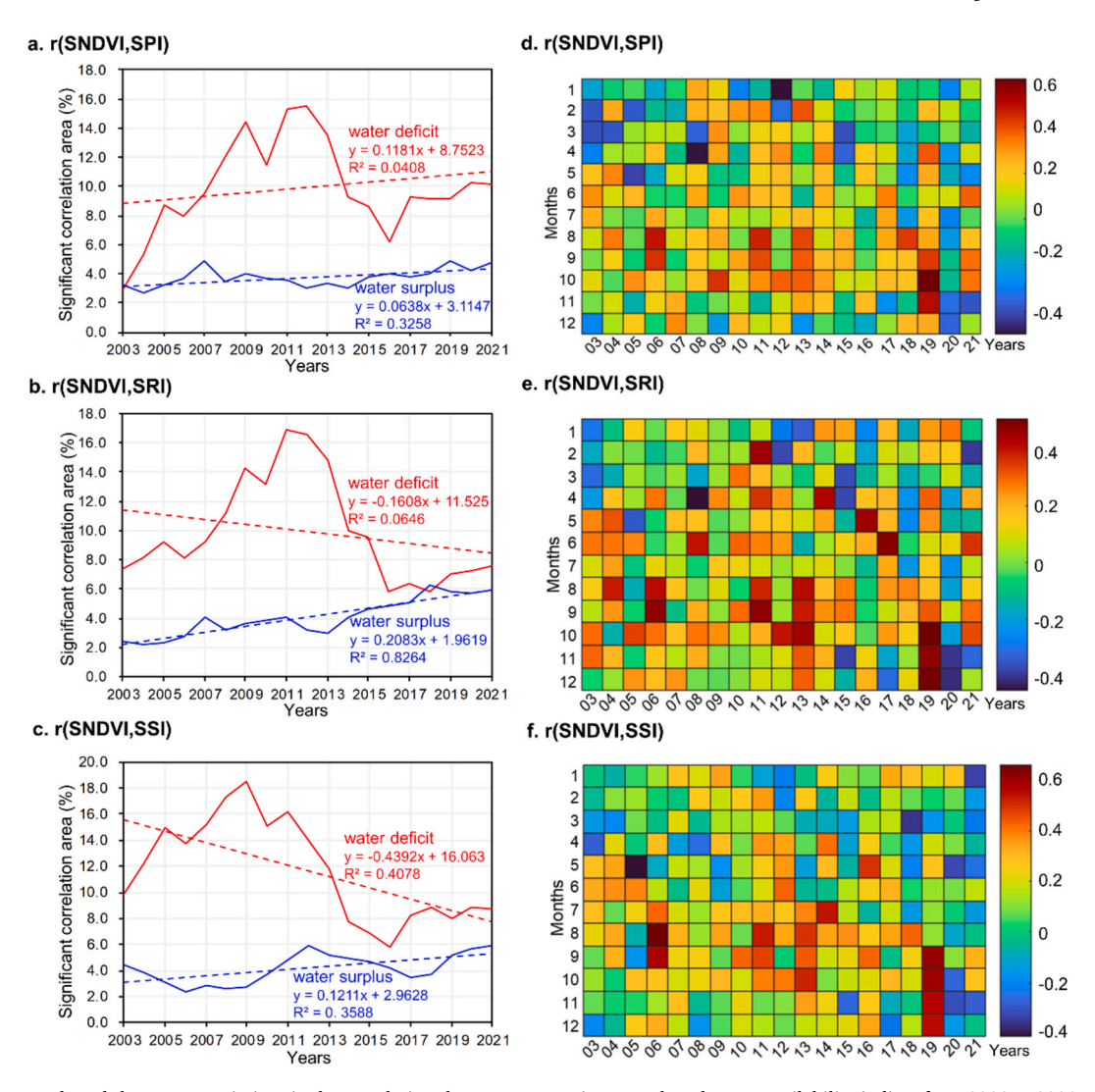


Fig. 3. Long-term trends and short-term variations in the correlations between vegetation growth and water availability indices from 2003 to 2021. Fig. 3a–c use a 5-year moving window to display the trends of significant correlation areas in subbasins. The red line represents vegetation growth hindered by water scarcity (r > 0), whereas the blue line represents that prevented by water scarcity (r < 0). Fig. 3d–f present the r(SNDVI, SPI), r(SNDVI, SRI), and r(SNDVI, SSI) through heatmaps, where strongly positive values are depicted in dark red and highly negative values are depicted in navy blue.

River basin, r(SNDVI, SRI) displayed a stronger positive correlation, with its highest value at 0.47 (Fig. 4a-c).

Moving towards the middle and lower YRB, moderate positive correlations were observed in both the southern and northeastern regions, with r-values of approximately 0.30 (Fig. 4a–c). In the southern part of the middle YRB, r(SNDVI, SRI) exhibited a contiguous distribution of relatively high values, peaking at approximately 0.37 in a sub-basin (Fig. 4b). This value was higher than the maximum r(SNDVI, SPI) and r(SNDVI, SSI) values, which were approximately 0.36 and 0.23, respectively (Fig. 4a and c). In the northeastern part of the lower YRB, r (SNDVI, SSI) also showed a contiguous cluster of relatively high values (approximately 0.40), extending into the northern Poyang Lake basin (Fig. 4c). Furthermore, in the middle and lower reaches of the YRB, an increasing trend was observed in r(SNDVI, SPI), r(SNDVI, SRI), and r (SNDVI, SSI), particularly in the Dongting Lake basin (Fig. 4g-i). Moreover, in the southeastern parts of the YRB, such as the Poyang Lake basin, decreasing trends were observed in r(SNDVI, SRI) and r(SNDVI, SSI) (Fig. 4h and i).

4.3. Analysis of the impact of different drought types on vegetation

Using the BRT model, we conduct an analysis of the contributions of

the SRI, SSI, and SPI to the NDVI anomalies (SNDVI) (Fig. 5). We find that the contributions of the three available water indices to vegetation growth, from highest to lowest, are the SRI (50 %), SSI (40 %), and SPI (10 %) (Fig. 5a). Specifically, the impact of the SPI on the SNDVI variation is relatively small compared to the SRI and SSI (Fig. 5b). Additionally, when SPI, SRI, and SSI increase from -2 to nearly 0, the marginal effect curves of SNDVI exhibit stepwise increases, with these increases becoming more gradual after reaching 0 (Fig. 5b–d). As for the marginal effects of SRI and SSI, the shapes of the curves are similar, though their inflection points differ: the former is located to the right of -1, while the latter is located to the left of -1 (Fig. 5c and d).

5. Discussion

5.1. Comparison of vegetation responses to water constraints

We compared the responses of vegetation anomalies to water constraints in the YRB, analyzing how water deficit and surplus limitations from diverse sources—precipitation, runoff, and soil moisture—affect vegetation growth across long-term, monthly, and spatial dynamics. The long-term response trends of vegetation anomalies to precipitation, runoff, and soil moisture surpluses or deficits differ from 2003 to 2021.

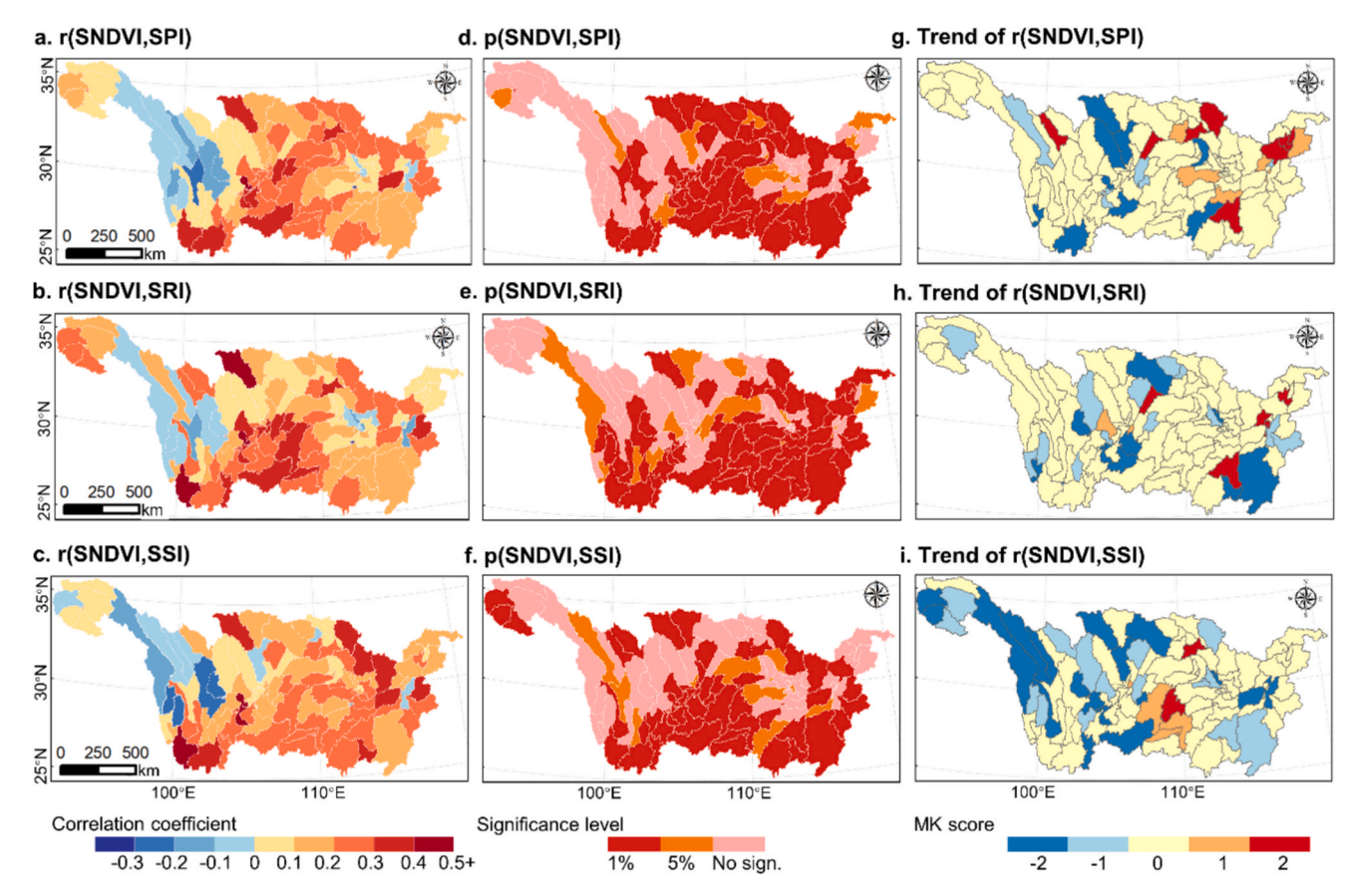


Fig. 4. Spatial distributions, significance and trends of vegetation–water correlations in the YRB. Fig. 4a–c show the spatial distributions of the correlations between the SPI, SRI, and SSI and the SNDVI. Fig. 4d–f present the significance levels. Fig. 4g–i show the spatial dispersal of the coefficients in the MK trend, where the absolute values of the MK scores in "2" and "1" separately reflect strong (above 99 % confidence) and moderate (between 95 % and 99 % confidence) extents. The positive mark is growth (filled in red), and the negative mark is reduction (in blue). There was no significant trend (in yellow), and the grade was "0".

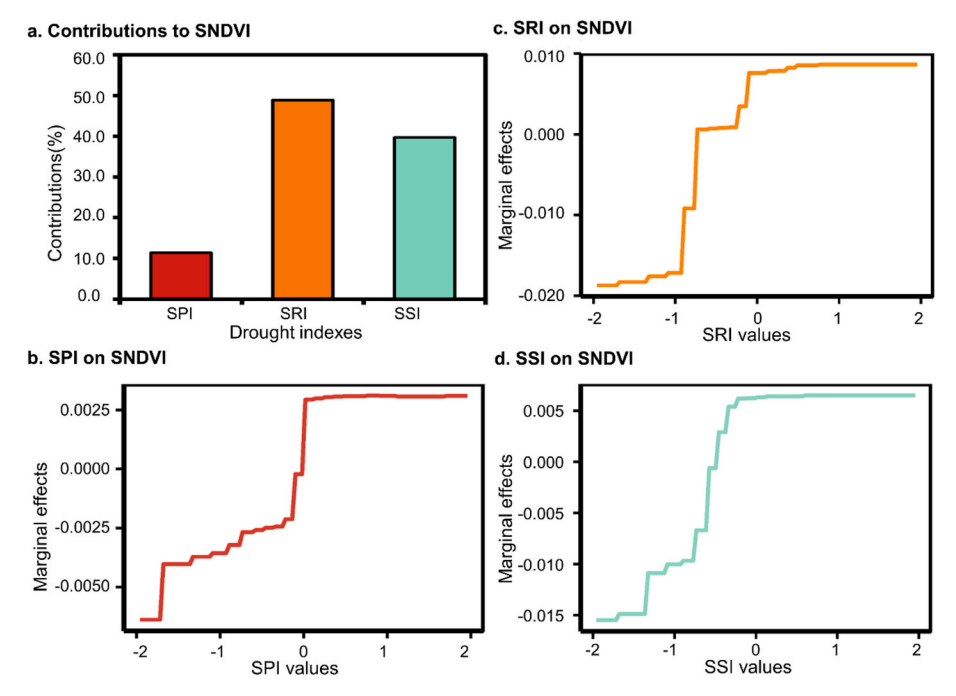


Fig. 5. The impact of three available water sources on vegetation dynamics. In Fig. 5a, the contributions of the SPI, SRI and SSI to the SNDVI are shown, summing to 100%. Fig. 5b-d depict the marginal effects of the SPI, SRI and SSI on the SNDVI. The independent variables are the SPI, SRI, and SSI, whereas the dependent variable is the SNDVI.

Only the positive correlation in the r(SNDVI, SPI) shows an increasing trend, indicating that vegetation growth is becoming increasingly limited by extended precipitation deficits, which may result from a reduction in precipitation frequency across the basin (Hu et al., 2021; Zhang et al., 2023b). However, the positive correlation in the r(SNDVI, SRI) and r(SNDVI, SSI) shows a decreasing trend in the YRB, indicating that the constraints of runoff and soil moisture deficiency on vegetation productivity are decreasing. This change may be related to the broader role of hydraulic infrastructure, such as the Three Gorges and Xiangjiaba Dams, which potentially mitigated soil moisture and runoff shortages, thereby alleviating water scarcity constraints on vegetation. In contrast, the most significant increase in the negative correlation of r(SNDVI, SRI) indicates that vegetation is increasingly constrained by runoff surpluses, likely due to rising frequency of extreme rainfall events that intensify waterlogging effects (Li et al., 2021).

The monthly correlation patterns reveal seasonal responses of vegetation to surplus and deficit constraints from diverse water sources. From April to October, the predominantly positive correlations between SNDVI and available water indices suggest that water deficits constrain vegetation growth during the growing season. Specifically, positive correlations observed during periods such as July to September 2006, August to October 2011, and September to December 2019 are consistent with drought events identified in previous studies (Wang et al., 2020; Liu et al., 2023), and support the concept of "vegetation water deficit restriction". Among these periods, the positive r(SNDVI, SRI) persisted for the longest duration, indicating that runoff shortage exerts a longer-lasting detriment to vegetation growth. Additionally, the positive r(SNDVI, SSI) exhibited relatively high correlations, indicating that among diverse water sources, soil moisture scarcity has a greater limiting effect on vegetation growth. However, in exceptional cases during the growing season, negative correlations between SNDVI and available water indices were observed, suggesting that water surpluses limit vegetation dynamics. For example, the negative correlations observed from May to December 2020, coinciding with significant flooding (Zhou et al., 2021; Wei et al., 2020), validate the "vegetation water surplus limitation" concept. During this period, the negative correlation of r(SNDVI, SSI) persisted for the longest duration, indicating that soil moisture surplus exerts more enduring negative impacts and that such limitations exhibit more stable characteristics. Moreover, the negative r(SNDVI, SRI) showed a stronger negative correlation, indicating that among diverse water sources, runoff surplus imposes a greater limitation on vegetation growth.

The spatial responses of vegetation to water constraints vary, with regional differences in the surplus or deficit limitations imposed by specific water sources. In the upper YRB, r(SNDVI, SSI) showed a stronger negative correlation compared to r(SNDVI, SPI) and r(SNDVI, SRI), indicating that vegetation health is more adversely affected by soil moisture surplus. Furthermore, decreasing trends in r(SNDVI, SSI) were observed in a patchy distribution across the Jinsha River basins, indicating that vegetation growth tends to be restricted by the soil moisture surplus, which aligns with the findings of Sun et al. (2022) of lower agricultural drought intensity and frequency in Southwest China. In contrast, in the Source Region of the Yangtze River, stronger positive correlations were observed in r(SNDVI, SPI) and r(SNDVI, SRI), whereas r(SNDVI, SSI) showed a weak positive correlation, indicating that vegetation vitality is more constrained by precipitation and runoff deficits. In the middle and lower YRB, an increasing trend between SNDVI and available water indices was observed, particularly in the Dongting Lake basin. This indicates that vegetation growth is increasingly constrained by water scarcity; possibly resulting from earlier exposure of wetlands and runoff interception by the Three Gorges Reservoir (Huang et al., 2014). In contrast, in the southeastern parts of the YRB, such as the Poyang Lake basin, decreasing trends were observed in r(SNDVI, SRI) and r(SNDVI, SSI), implying that vegetation is increasingly hindered by water surplus, consistent with the rising hydrological impacts of flood disasters (Li and Zhang, 2015). In the southern part of the middle YRB,

high positive r(SNDVI, SRI) exhibited a contiguous distribution, indicating that vegetation is primarily affected by runoff shortage. Meanwhile, in the northeastern part of the lower YRB, high positive r(SNDVI, SSI) also showed a contiguous cluster, suggesting that soil moisture shortage plays a major role in limiting vegetation growth.

Interestingly, unlike studies emphasizing soil moisture and precipitation in vegetation dynamics (Lawal et al., 2019; Du et al., 2023), our results highlight the critical role of runoff in the YRB. Several key mechanisms are likely to explain these findings. First, unlike drought-resistant vegetation, which allocates significant nutrients to root development (Chaturvedi et al., 2021), plants in nonarid lands of the YRB invest less in their root systems. Furthermore, while vegetation root systems play crucial roles in water infiltration (Wu et al., 2016), the heterogeneous distribution of terrain and soil composition often hinders surface runoff from penetrating the soil in certain areas of a basin (Daly and Porporato, 2005), causing reduced soil moisture levels (Cui et al., 2022) and challenges for vegetation in accessing soil moisture. Consequently, while soil moisture influences vegetation health (Seka et al., 2022), direct water supply from runoff may exert a more significant influence.

5.2. Implications for management and future studies

In light of these insights, comprehensive water resource management strategies are imperative to ensure the resilience of vegetation growth and ecosystem functionality in the YRB. To scientifically regulate water resource allocation within the basin, rational use of reservoirs, water diversion, and regulation projects is essential (Guo et al., 2021). Therefore, effective water resource management schemes should be tailored regionally, considering local factors affecting vegetation growth. Specifically, in the upper Jinsha River, particularly in western Sichuan Province, improving soil drainage is crucial to mitigate the impact of excess soil moisture on vegetation. Meanwhile, in the upper YRB, which are expected to face more severe hydrological droughts (Liang et al., 2023), water conservation practices and efficient irrigation systems are vital to address vegetation growth constraints caused by precipitation and runoff deficits. In the southeastern parts of the YRB, integrated water management strategies, including optimized runoff regulation and targeted irrigation, are necessary to ensure sustainable vegetation growth (Xu et al., 2020).

This study offers insights that could inform future research on the interaction of diverse water sources and vegetation anomalies in the YRB. First, we employed the SWAT model to obtain soil moisture data, which ranges from 0 to 100 cm and is closely related to the vegetation root zone growth. However, future work could incorporate a more diverse dataset, such as remote sensing soil moisture data at a depth of 0-5 cm. This integration would offer a more comprehensive understanding of soil moisture dynamics. Second, we used SNDVI to capture vegetation anomalies under water stress, enabling us to analyze vegetation responses to drought at a large basin scale. Future research could incorporate land use patterns to conduct more detailed studies on representative land cover types, such as forests, grasslands, and croplands, and their water limitations, including precipitation, runoff, and soil moisture deficit or surplus. Given the complex relationships between available water indices (SPI, SRI, and SSI) and SNDVI, future work could focus on refining models that integrate multiple indices with vegetation health indicators. This would improve understanding of how different drought types impact vegetation over various time scales, with particular attention to seasonal fluctuations during critical growing periods. As climate change increases the frequency of extreme weather events, research could incorporate climate projections to assess the impact of future droughts on vegetation in the YRB.

6. Conclusion

The findings of this study underscore the interplay of

water-vegetation systems in the YRB, revealing that vegetation ecosystem stability is affected by water constraints. Through an analysis of water-vegetation interactions from 2003–2021, several key conclusions have been drawn:

- (1) More areas in the YRB are affected by water shortages than surpluses in terms of vegetation growth. The constraints of runoff and soil moisture deficiency on vegetation vitality are decreasing, while the restrictions due to water surplus, particularly runoff surplus, have gradually increased in the YRB. Vegetation faces diverse water limitations across seasonal growth periods. During the growing season, vegetation is primarily affected by water shortage, although in exceptional cases, it is constrained by excess water, which typically occurs during the nongrowing season. The negative impact of runoff scarcity and soil moisture surplus on greenery health are more enduring.
- (2) In the upper and middle Jinsha River Basin and the western Min River Basin, vegetation growth is primarily restricted by soil moisture surplus, while in the southern Jinsha River Basin, soil moisture deficits impose even greater limitations. In the Source Region of the Yangtze River and the northwestern Jialing River basin, it is mainly driven by precipitation and runoff deficits. In the southern part of the middle YRB, vegetation is more constrained by runoff surplus, whereas in the northeastern part of the lower YRB, soil moisture surplus has a stronger impact. In the southeastern YRB, including the Poyang Lake basin, vegetation growth tends to be constrained by water surplus.
- (3) In the YRB, runoff (SRI) and soil moisture (SSI) play more significant roles in influencing vegetation growth than does precipitation (SPI). The improved vegetation conditions primarily stem from the alleviation of hydrological drought, which has a substantial impact on vegetation growth. Vegetation is highly sensitive to hydrological and agricultural drought, with improvements in vegetation occurring as drought conditions are slightly alleviated.

CRediT authorship contribution statement

Sijing Cui: Writing – review & editing, Writing – original draft, Visualization, Methodology, Conceptualization. Jun Gao: Project administration, Formal analysis, Conceptualization. Fengyun Sun: Writing – review & editing, Validation, Supervision, Software, Resources, Methodology, Funding acquisition, Formal analysis. Gen Li: Project administration, Investigation, Formal analysis. Yue Che: Funding acquisition, Formal analysis.

Declaration of competing interest

The authors declare that they have no known competing financial interests or personal relationships that could have appeared to influence the work reported in this paper.

Acknowledgements

This work is supported by the National Science Foundation for Young Scientists of China (Grant No. 42007417), and the Science and Technology Commission of Shanghai Municipality (Grant No. 23002400400).

Data availability

Data will be made available on request.

References

- Abbaspour, K.C., Rouholahnejad, E., Vaghefi, S., Srinivasan, R., Yang, H., Kløve, B., 2015. A continental-scale hydrology and water quality model for Europe: calibration and uncertainty of a high-resolution large-scale SWAT model. J. Hydrol. 524, 733–752. https://doi.org/10.1016/j.jhydrol.2015.03.027.
- Allen, C.D., Breshears, D.D., McDowell, N.G., 2015. On underestimation of global vulnerability to tree mortality and forest die-off from hotter drought in the Anthropocene. Ecosphere 6 (8), 1–55. https://doi.org/10.1890/E\$15-00203.1.
- Anderegg, W.R., Konings, A.G., Trugman, A.T., Yu, K., Bowling, D.R., Gabbitas, R., Karp, D.S., Pacala, S., Sperry, J.S., Sulman, B.N., 2018. Hydraulic diversity of forests regulates ecosystem resilience during drought. Nature 561, 538–541. https://doi.org/10.1038/s41586-018-0539-7.
- Arnold, J.G., Moriasi, D.N., Gassman, P.W., Abbaspour, K.C., White, M.J., Srinivasan, R., Santhi, C., Harmel, R., Van Griensven, A., Van Liew, M.W., 2012. SWAT: model use, calibration, and validation. Trans. ASABE. 55(4), 1491–1508. doi: 10.13031/2013.42256.
- Blom, C.W.P.M., 1999. Adaptations to flooding stress: from plant community to molecule. Plant Biol. (Stuttg.) 1 (3), 261–273. https://doi.org/10.1111/j.1438-8677.1999 tb00252 x
- Chaturvedi, R.K., Tripathi, A., Raghubanshi, A.S., Singh, J.S., 2021. Functional traits indicate a continuum of tree drought strategies across a soil water availability gradient in a tropical dry forest. For. Ecol. Manage. 482, 118740. https://doi.org/ 10.1016/j.fprecp.2020.118740.
- Chang, Q., He, H., Ren, X., Zhang, L., Feng, L., Lv, Y., Zhang, M., Xu, Q., Liu, W., Zhang, Y., Wang, T., 2023. Soil moisture drives the spatiotemporal patterns of asymmetry in vegetation productivity responses across China. Sci. Total Environ. 855, 158819. https://doi.org/10.1016/j.scitotenv.2022.158819.
- Chen, F., Crow, W.T., Starks, P.J., Moriasi, D.N., 2011. Improving hydrologic predictions of a catchment model via assimilation of surface soil moisture. Adv. Water Resour. 34 (4), 526–536. https://doi.org/10.1016/j.advwatres.2011.01.011.
- Cui, Z., Huang, Z., Liu, Y., López-Vicente, M., Wu, G.-L., 2022. Natural compensation mechanism of soil water infiltration through decayed roots in semi-arid vegetation species. Sci. Total Environ. 819, 151985. https://doi.org/10.1016/j. scitoteny 2021 151985
- Daly, E., Porporato, A., 2005. A review of soil moisture dynamics: from rainfall infiltration to ecosystem response. Environ. Eng. Sci. 22 (1), 9–24. https://doi.org/ 10.1089/ees.2005.22.9.
- De'ath, G., 2007. Boosted trees for ecological modeling and prediction. Ecology 88 (1), 243–251. https://doi.org/10.1890/0012-9658(2007)88[243:btfema]2.0.co;2.
- Douglas-Mankin, K., Srinivasan, R., Arnold, J., 2010. Soil and Water Assessment Tool (SWAT) model: current developments and applications. Trans. ASABE. 53(5), 1423-1431. doi: 10.13031/2013.34915.
- Du, R., Wu, J., Tian, F., Yang, J., Han, X., Chen, M., Zhao, B., Lin, J., 2023. Reversal of soil moisture constraint on vegetation growth in North China. Sci. Total Environ. 865, 161246. https://doi.org/10.1016/j.scitotenv.2022.161246.
- FAO, 2020. Global Forest Resources Assessment 2020: main report. FAO Knowledge Repository BETA, Rome. doi: 10.4060/ca9825en.
- Farahmand, A., AghaKouchak, A., 2015. A generalized framework for deriving nonparametric standardized drought indicators. Adv. Water Resour. 76, 140–145. https://doi.org/10.1016/j.advwatres.2014.11.012.
- Gassman, P.W., Reyes, M.R., Green, C.H., Arnold, J.G., 2007. The soil and water assessment tool: historical development, applications, and future research directions. Trans. ASABE. 50(4), 1211-1250. doi: 10.13031/2013.23637.
- Guo, S., Xiong, L., Zha, X., Zeng, L., Cheng, L., 2021. Impacts of the Three Gorges Dam on the streamflow fluctuations in the downstream region. J. Hydrol. 598, 126480. https://doi.org/10.1016/j.jhydrol.2021.126480.
- Hauke, J., Kossowski, T., 2011. Comparison of values of Pearson's and Spearman's correlation coefficients on the same sets of data. Quaest. Geogr. 30 (2), 87–93. https://doi.org/10.2478/v10117-011-0021-1.
- Huang, Q., Sun, Z., Opp, C., Lotz, T., Jiang, J., Lai, X., 2014. Hydrological drought at Dongting Lake: its detection, characterization, and challenges associated with Three Gorges Dam in Central Yangtze China. Water Resour. Manag. 28, 5377–5388. https://doi.org/10.1007/s11269-014-0807-8.
- Humphrey, V., Zscheischler, J., Ciais, P., Gudmundsson, L., Sitch, S., Seneviratne, S.I., 2018. Sensitivity of atmospheric CO₂ growth rate to observed changes in terrestrial water storage. Nature 560, 628–631. https://doi.org/10.1038/s41586-018-0424-4.
- Hu, M., Dong, M., Tian, X., Wang, L., Jiang, Y., 2021. Trends in different grades of precipitation over the Yangtze River Basin from 1960 to 2017. Atmos. 12 (3), 413. https://doi.org/10.3390/atmos12030413.
- Ji, L., Peters, A.J., 2003. Assessing vegetation response to drought in the northern Great Plains using vegetation and drought indices. Remote Sens. Environ. 87 (1), 85–98. https://doi.org/10.1016/S0034-4257(03)00174-3.
- Ji, Y., Fu, J., Liu, B., Tan, X., 2024. Can limiting global temperature rise to below 2° C warming prevent the emergence of unprecedented drought? Agric. For. Meteorol. 352, 110047. https://doi.org/10.1016/j.agrformet.2024.110047.
- Jiao, W., Wang, L., Smith, W.K., Chang, Q., Wang, H., D'Odorico, P., 2021. Observed increasing water constraint on vegetation growth over the last three decades. Nat. Commun. 12, 3777. https://doi.org/10.1038/s41467-021-24016-9.
- Juglea, S., Kerr, Y., Mialon, A., Lopez-Baeza, E., Braithwaite, D., Hsu, K., 2010. Soil moisture modelling of a SMOS pixel: interest of using the PERSIANN database over the Valencia Anchor Station. Hydrol. Earth Syst. Sci. 14 (8), 1509–1525. https://doi.org/10.5194/hess-14-1509-2010.
- Jung, M., Reichstein, M., Ciais, P., Seneviratne, S.I., Sheffield, J., Goulden, M.L., Bonan, G., Cescatti, A., Chen, J., De Jeu, R., Dolman, A.J., 2010. Recent decline in

- the global land evapotranspiration trend due to limited moisture supply. Nature 467, 951–954. https://doi.org/10.1038/nature09396.
- Kendall, M.G., 1975. Rank Correlation Measure. Charles Griffin, London.
- Kreuzwieser, J., Rennenberg, H., 2014. Molecular and physiological responses of trees to waterlogging stress. Plant Cell Environ. 37, 2245–2259. https://doi.org/10.1111/ pce_12310
- Lawal, S., Lennard, C., Jack, C., Wolski, P., Hewitson, B., Abiodun, B., 2019. The observed and model-simulated response of southern African vegetation to drought. Agric. For. Meteorol. 279, 107698. https://doi.org/10.1016/j. agrformet.2019.107698.
- Liang, H., Zhang, D., Wang, W., Yu, S., Nimai, S., 2023. Evaluating future water security in the upper Yangtze River Basin under a changing environment. Sci. Total Environ. 889, 164101. https://doi.org/10.1016/j.scitotenv.2023.164101.
- Li, X., Zhang, Q., 2015. Variation of floods characteristics and their responses to climate and human activities in Poyang Lake. China. Chin. Geogr. Sci. 25, 13–25. https:// doi.org/10.1007/s11769-014-0724-z.
- Li, X., Zhang, K., Gu, P., Feng, H., Yin, Y., Chen, W., Cheng, B., 2021. Changes in precipitation extremes in the Yangtze River Basin during 1960–2019 and the association with global warming, ENSO, and local effects. Sci. Total Environ. 760, 144244. https://doi.org/10.1016/j.scitotenv.2020.144244.
- Li, Z., Liu, W.Z., Zhang, X.C., Zheng, F.L., 2009. Impacts of land use change and climate variability on hydrology in an agricultural catchment on the Loess Plateau of China. J. Hydrol. 377 (1–2), 35–42. https://doi.org/10.1016/j.jhydrol.2009.08.007.
- Liu, Y., Yuan, S., Zhu, Y., Ren, L., Chen, R., Zhu, X., Xia, R., 2023. The patterns, magnitude, and drivers of unprecedented 2022 mega-drought in the Yangtze River Basin, China. Environ. Res. Lett. 18 (11), 114006. https://doi.org/10.1088/1748-9326/acfe21.
- McKee, T.B., Doesken, N.J., Kleist, J., 1993. The relationship of drought frequency and duration to time scales. Proc. 8th Conf. Appl. Clim. 17 (22), 179–183.
- Meroni, M., Fasbender, D., Rembold, F., Atzberger, C., Klisch, A., 2019. Near real-time vegetation anomaly detection with MODIS NDVI: timeliness vs. accuracy and effect of anomaly computation options. Remote Sens. Environ. 221, 508–521. https://doi. org/10.1016/j.rse.2018.11.041.
- Mishra, A.K., Singh, V.P., 2010. A review of drought concepts. J. Hydrol. 391 (1–2), 202–216. https://doi.org/10.1016/j.jhydrol.2010.07.012.
- Mitchell, P.J., O'Grady, A.P., Pinkard, E.A., Brodribb, T.J., Arndt, S.K., Blackman, C.J., Duursma, R.A., Fensham, R.J., Hilbert, D.W., Nitschke, C.R., Norris, J., 2016. An ecoclimatic framework for evaluating the resilience of vegetation to water deficit. Glob. Chang. Biol. 22, 1677–1689. https://doi.org/10.1111/gcb.13177.
- Nemani, R.R., Keeling, C.D., Hashimoto, H., Jolly, W.M., Piper, S.C., Tucker, C.J., Myneni, R.B., Running, S.W., 2003. Climate-driven increases in global terrestrial net primary production from 1982 to 1999. Science 300, 1560–1563. https://doi.org/ 10.1126/science.1082750.
- Peña -Angulo, D., Vicente-Serrano, S.M., Domínguez-Castro, F., Noguera, I., Tomas-Burguera, M., López-Moreno, J.I., 2021. Unravelling the role of vegetation on the different trends between climatic and hydrologic drought in headwater catchments of Spain. Anthropocene 36, 100309. doi: 10.1016/j.ancene.2021.100309.
- Qu, S., Wang, L., Lin, A., Yu, D., Yuan, M., 2020. Distinguishing the impacts of climate change and anthropogenic factors on vegetation dynamics in the Yangtze River Basin, China. Ecol. Ind. 108, 105724. https://doi.org/10.1016/j. ecolind 2019 105724
- Reichstein, M., Ciais, P., Papale, D., Valentini, R., RUNNING, S., Viovy, N., Cramer, W., Granier, A., Ogée, J., Allard, V., 2007. Reduction of ecosystem productivity and respiration during the European summer 2003 climate anomaly: a joint flux tower, remote sensing and modelling analysis. Glob. Chang. Biol. 13, 634-651. doi: 10.1111/j.1365-2486.2006.01224.x.
- Schober, P., Boer, C., Schwarte, L.A., 2018. Correlation coefficients: appropriate use and interpretation. Anesth. Analg. 126 (5), 1763–1768. https://doi.org/10.1213/ ANE.0000000000002864.
- Schwalm, C.R., Anderegg, W.R., Michalak, A.M., Fisher, J.B., Biondi, F., Koch, G., Litvak, M., Ogle, K., Shaw, J.D., Wolf, A., Huntzinger, D.N., 2017. Global patterns of drought recovery. Nature 548, 202–205. https://doi.org/10.1038/nature23021.
- Seka, A.M., Zhang, J., Prodhan, F.A., Ayele, G.T., Finsa, M.M., Sharma, T.P.P., Melesse, A.M., 2022. Hydrological drought impacts on water storage variations: a focus on the role of vegetation changes in the East Africa region. A Systematic Review. Environ. Sci. Pollut. 29 (53), 80237–80256. https://doi.org/10.1007/ s11356-022-23313-0.

- Smith, T., Boers, N., 2023. Global vegetation resilience linked to water availability and variability. Nat. Commun. 14 (1), 498. https://doi.org/10.1038/s41467-023-36207-7
- Sperry, J.S., Love, D.M., 2015. What plant hydraulics can tell us about responses to climate-change droughts. New Phytol. 207 (1), 14–27. https://doi.org/10.1111/ nph.13354.
- Sun, F., Mejia, A., Zeng, P., Che, Y., 2019. Projecting meteorological, hydrological and agricultural droughts for the Yangtze River basin. Sci. Total Environ. 696, 134076. https://doi.org/10.1016/j.scitotenv.2019.134076.
- Sun, X., Lai, P., Wang, S., Song, L., Ma, M., Han, X., 2022. Monitoring of extreme agricultural drought of the past 20 years in southwest China using GLDAS soil moisture. Remote Sens. 14 (6), 1323. https://doi.org/10.3390/rs14061323.
- Tang, J., Niu, B., Hu, Z., Zhang, X., 2024. Increasing susceptibility and shortening response time of vegetation productivity to drought from 2001 to 2021. Agric. For. Meteorol. 352, 110025. https://doi.org/10.1016/j.agrformet.2024.110025.
- Wang, J., Chen, Y., Wang, Z., Shang, P., 2020. Drought evaluation over Yangtze River basin based on weighted water storage deficit. J. Hydrol. 591, 125283. https://doi. org/10.1016/j.jhydrol.2020.125283.
- Wang, M., Ding, Z., Wu, C., Song, L., Ma, M., Yu, P., Lu, B., Tang, X., 2021a. Divergent responses of ecosystem water-use efficiency to extreme seasonal droughts in Southwest China. Sci. Total Environ. 760, 143427. https://doi.org/10.1016/j. scitotenv.2020.143427.
- Wang, H., Li, Z., Cao, L., Feng, R., Pan, Y., 2021b. Response of NDVI of natural vegetation to climate changes and drought in China. Land 10 (9), 966. https://doi.org/ 10.1016/10.3390/land10090966
- Wei, K., Ouyang, C., Duan, H., Li, Y., Chen, M., Ma, J., An, H., Zhou, S., 2020. Reflections on the catastrophic 2020 Yangtze River Basin flooding in southern China. Innovation (camb) 1 (2). https://doi.org/10.1016/j.xinn.2020.100038.
- Wu, G.L., Yang, Z., Cui, Z., Liu, Y., Fang, N.F., Shi, Z.H., 2016. Mixed artificial grasslands with more roots improved mine soil infiltration capacity. J. Hydrol. 535, 54–60. https://doi.org/10.1016/j.jhydrol.2016.01.059.
- Wu, W., Li, C., Liu, M., Hu, Y., Xiu, C., 2020. Change of impervious surface area and its impacts on urban landscape: an example of Shenyang between 2010 and 2017. Ecosyst. Health Sust. 6 (1), 1767511. https://doi.org/10.1080/ 20964129.2020.1767511.
- Xu, D., Lyon, S.W., Mao, J., Dai, H., Jarsjö, J., 2020. Impacts of multi-purpose reservoir construction, land-use change and climate change on runoff characteristics in the Poyang Lake basin. China. J. Hydrol. Reg. Stud. 29, 100694. https://doi.org/ 10.1016/i.eirh.2020.100694.
- Yang, Y., Donohue, R.J., McVicar, T.R., 2016. Global estimation of effective plant rooting depth: implications for hydrological modeling. Water Resour. Res. 52 (10), 8260–8276. https://doi.org/10.1002/2016WR019392.
- Yang, Y., Wang, Y., Cong, N., Wang, N., Yao, W., 2024. Impacts of the Three Gorges Dam on riparian vegetation in the Yangtze River Basin under climate change. Sci. Total Environ. 912, 169415. https://doi.org/10.1016/j.scitotenv.2023.169415.
- Yu, G., Chen, Z., Piao, S., Peng, C., Ciais, P., Wang, Q., Li, X., Zhu, X., 2014. High carbon dioxide uptake by subtropical forest ecosystems in the East Asian monsoon region. Proc. Nat. Acad. Sci. 111 (13), 4910–4915. https://doi.org/10.1073/pnas.1317065111.
- Zhang, C., Sun, F., Sharma, S., Zeng, P., Mejia, A., Lyu, Y., Gao, J., Zhou, R., Che, Y., 2023a. Projecting multi-attribute flood regime changes for the Yangtze River basin. J. Hydrol. 617, 128846. https://doi.org/10.1016/j.jhydrol.2022.128846.
- Zhang, C., Xiao, C., Li, S., Sangbu, C., Ren, Y., Zhang, S., Wang, R., 2023b. Construction of multi-extreme climate events composite grads index and comprehensive analysis of extreme climate in the Yangtze River Basin from 1961 to 2020. Chin. J. Geophys. 66 (3), 920–938. https://doi.org/10.6038/cjg2022Q0255.
- Zhang, J., Zhang, Y., Sun, G., Song, C., Li, J., Hao, L., Liu, N., 2022. Climate variability masked greening effects on water yield in the Yangtze River Basin during 2001–2018. Water Resour. Philos. Phenomenol. Res. 58 (1), e2021WR030382. https://doi.org/10.1029/2021WR030382.
- Zhang, Z., Chao, B.F., Chen, J., Wilson, C.R., 2015. Terrestrial water storage anomalies of Yangtze River Basin droughts observed by GRACE and connections with ENSO. Glob. Planet. Change 126, 35–45. https://doi.org/10.1016/j.gloplacha.2015.01.002.
- Zhou, Z.Q., Xie, S.P., Zhang, R.H., 2021. Historic Yangtze flooding of 2020 tied to extreme Indian Ocean conditions. Proc. Nat. Acad. Sci. 118 (12), e2022255118. https://doi.org/10.1073/pnas.2022255118.